The Proportional Integral Notch and Coleman Blade Effective Wind Speed Estimators and Their Similarities

Liu, Yichao; Pamososuryo, Atindriyo K.; Mulders, Sebastiaan P.; Ferrari, Riccardo M.G.; van Wingerden, Jan Willem

DOI
10.1109/LCSYS.2021.3140171

Publication date
2022

Document Version
Final published version

Published in
IEEE Control Systems Letters

The Proportional Integral Notch and Coleman Blade Effective Wind Speed Estimators and Their Similarities

Yichao Liu, Atindriyo K. Pamososuryo, Sebastiaan P. Mulders, Riccardo M. G. Ferrari, *Member, IEEE*, and Jan-Willem van Wingerden, *Senior Member, IEEE*

***Abstract*—The estimation of the rotor effective wind speed is used in modern wind turbines to provide advanced power and load control capabilities. However, with the ever increasing rotor sizes, the wind field over the rotor surface shows a higher degree of spatial variation. A single effective wind speed estimation therefore limits the attainable levels of load mitigation, and the estimation of the blade effective wind speed (BEWS) might present opportunities for improved load control. This letter introduces two novel BEWS estimator approaches: a proportional-integral-notch (PIN) estimator based on individual blade load measurements, and a Coleman estimator targeting the estimation in the nonrotating frame. Given the seeming disparities between these two estimators, the objective of this letter is to analyze the similarities between the approaches. It is shown that the PIN estimator, which is equivalent to the diagonal form of the Coleman estimator, is a simple but effective method to estimate the BEWS. The Coleman estimator, which takes the coupling effects between individual blades into account, shows a more well-behaved transient response than the PIN estimator.**

***Index Terms*—Blade effective wind speed estimation, estimator, wind turbine, Coleman transformation.**

I. Introduction

OVER the past decade, wind energy has grown exponentially in the global energy mix, benefiting from scientific advancement, reduced costs and governments' subsidy schemes. The Global Wind Energy Council (GWEC) reported that more than 90 GW of new wind power was deployed in 2020 [1], exhibiting a global growth of 53 % compared to 2019. This growth is partially driven by the fact that the physical dimensions of wind turbines dramatically increased, which resulted in a rising demand for optimization of wind turbine control systems.

For larger turbines, the wind inflow conditions over the rotor area demonstrate a high degree of spatial variability. As a result, the need for more accurate and granular wind speed information is becoming ever more prominent for the design of effective control algorithms. The wind speed measurement from the conventional anemometer – located downwind of the rotor at the back of the nacelle – is generally omitted in the control system, as it is a single point-wise measurement disturbed by rotor induction [2]. Therefore, a wind sensing technique providing an estimate of the effective wind inflow conditions by leveraging the wind turbine rotor as a generalized anemometer, is considered as a viable solution to address this challenge.

Wind sensing techniques are based on the idea that wind state changes are reflected by prior turbine knowledge, real-time measurements and control signals. For instance, the widely-used Immersion and Invariance (I&I) estimator [3], [4] exploits prior knowledge on the (aerodynamic) turbine properties, combined with an angular speed measurement and the applied generator torque control signal to estimate the rotor effective wind speed (REWS).

The previously mentioned method still returns a single point-wise estimate of the effective wind speed across the rotor disc. The increasingly common usage of load sensors on wind turbines however, forms an opportunity for more advanced wind speed estimation solutions. Such advanced estimation schemes facilitate feedforward(-feedback) control configurations [5], [6], advanced wind turbine control [7] and wake impingement detection [8], [9]. Bottasso *et al.* [8] developed a load-sensing approach to estimate the REWS, where several wind characteristics are estimated (e.g., wind shear and yaw misalignment). Liu *et al.* [9] proposed a subspace predictive repetitive estimator (SPRE) to identify the periodic wind flow on an individual blade, while also providing approximations on wind shear and wake impingement based on blade load measurements. Although the algorithm has proven to be very effective, the SPRE approach introduces significant delays in the blade effective wind speed (BEWS)

Manuscript received September 14, 2021; revised November 30, 2021; accepted December 20, 2021. Date of publication January 4, 2022; date of current version January 11, 2022. This work was supported in part by the Netherlands Organization for Scientific Research (NWO) through VIDI under Grant 17512, and in part by the European Union via a Marie Sklodowska-Curie Action (Project EDOWE) under Grant 835901. Recommended by Senior Editor V. Ugrinovskii. *(Corresponding author: Yichao Liu.)*

The authors are with the Delft Center for Systems and Control, Delft University of Technology, 2628 CD Delft, The Netherlands (e-mail: y.liu-17@tudelft.nl; a.k.pamososuryo@tudelft.nl; s.p.mulders@tudelft.nl; r.ferrari@tudelft.nl; j.w.vanwingerden@tudelft.nl).

Digital Object Identifier 10.1109/LCSYS.2021.3140171

estimation, thus making it less suitable for closed-loop control.

In this letter, two novel load-sensing approaches to estimate the periodic wind flow on an individual blade are proposed. The first method is called proportional-integral-notch (PIN) estimator, in which an azimuth-dependent cone coefficient is defined to reflect the one-to-one relation between the wind speeds and the blade loads. It is also assumed that the periodic wind speed on an individual blade is a superposition of REWS and zero-mean BEWS acting on the rotating frequencies. The proportional-integral component of the estimator is used to estimate the REWS component at the nonrotating frequency, while the gain-scheduled notch is added to identify the zero-mean BEWS component at higher frequencies. The second approach employs the Coleman transformation to translate blade load signals from the rotating frame into the fixed frame. This transformation is often used in individual pitch control (IPC) implementations for blade fatigue load reductions [10]. The Coleman estimation technique shows resemblance with the PIN estimator, making it compelling to understand the similarities of both schemes in terms of their structure and performance. To this end, as a core contribution of this letter, a frequency-domain analysis has been performed to understand the similarities under varying wind conditions.

This letter provides the following contributions:

1) Proposing a novel PIN estimator to estimate the BEWS for wind turbines.
2) Accounting for the coupled blade dynamics by developing a new Coleman estimator.
3) Showcasing the similarities between the PIN and the Coleman estimators via theoretical analyses and numerical simulations.

The remainder of this letter is organized as follows: Section II introduces the wind turbine model considered in this letter and the azimuth-dependent cone coefficient used by the proposed wind speed estimators. Section III theoretically formalizes the estimation techniques and demonstrates the similarities of both schemes. In Section IV, high-fidelity wind turbine simulations are carried out to demonstrate the estimators' performance and to verify the theoretical results. Finally, conclusions are drawn in Section V.

II. Wind Turbine Model and Its Cone Coefficient

This section introduces the wind turbine model and the *azimuth-dependent cone coefficient* [8] which are used to establish the wind speed estimation schemes. For a horizontal axis wind turbine, the *azimuth-dependent cone coefficient* is defined as:

$$C_{\mathrm{m},i}(\lambda_i, q_i, \psi_i) \coloneqq \frac{m_i(\lambda_i, q_i, \psi_i)}{\frac{1}{2}\rho A R U_i^2}, \tag{1}$$

where ρ is the air density, A the rotor swept area, and U_i represents the BEWS. The *blade effective dynamic pressure* is given by:

$$q_i \coloneqq \frac{1}{2}\rho U_i^2. \tag{2}$$

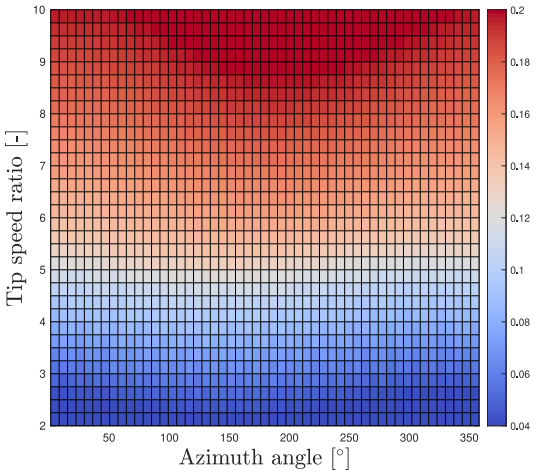

Fig. 1. Azimuth-dependent cone coefficient surface $C_{\mathrm{m},1}$ of the NREL 5-MW wind turbine model, obtained by steady-state simulations with a uniform constant wind speed of 8 m/s.

The measured out-of-plane blade root bending moment (MOoP) is denoted by m_i, which is – amongst other variables – a function of the azimuth angle $\psi_i = \psi + 2\pi(i-1)/3$, where $i = \{1, 2, 3\}$ is the blade index for a three-bladed wind turbine and ψ the azimuth angle of the first blade. The cone coefficient is represented by $C_{\mathrm{m},i}$ and depends on the azimuth position of blade i. Here, $C_{\mathrm{m},i}$ is a nonlinear function of the *tip-speed ratio*

$$\lambda_i \coloneqq \frac{\omega_{\mathrm{r}} R}{U_i}, \tag{3}$$

where ω_{r} and R are the rotor speed and the rotor radius, respectively. The shape of the $C_{\mathrm{m},i}$ surface is determined by the structural design of the wind turbine, and is typically derived via either high-fidelity numerical simulations or experimental tests. Note that $C_{\mathrm{m},i}$ is also a function of the blade pitch angle [9]. However, without loss of generality, the pitch angle is assumed to be constant throughout this letter. The cone coefficient can be extended for varying pitch angles by including an additional dependency on that parameter.

The wind turbine model considered in this letter is the National Renewable Energy Laboratory (NREL) 5-MW reference wind turbine [11]. Its $C_{\mathrm{m},1}$ curve is shown in Fig. 1 for illustration purposes, which is obtained from steady-state wind turbine simulations, in which the turbine is subjected to a uniform wind condition with a constant velocity of 8 m/s.

Once the cone coefficient is derived for each blade and over the operating conditions of interests, Eq. (1) can be used to estimate the MOoP according to $\hat{U}_i$ as:

$$\hat{m}_i(\lambda_i, q_i, \psi_i) = \frac{1}{2}\rho A R \hat{U}_i^2 C_{\mathrm{m},i}(\lambda_i, q_i, \psi_i). \tag{4}$$

Based on the wind turbine model and its azimuth-dependent cone coefficient, the BEWS estimator problem is formalized in Section III.

III. Blade Effective Wind Speed Estimator

First, the following assumptions are formulated for the wind speed estimation problem.

Assumption 1: The blade effective wind speeds for an individual blade U_i and for the rotor disk $\bar{U}$ are regarded as positive and *unknown* signals.

Assumption 2: The signals m_i and ω_r are assumed to be measured. The wind turbine operates at a constant rotor speed, i.e., $\dot{\omega}_\mathrm{r}(t) = 0$.

The wind speed estimation problem solved in this letter is thus formulated as:

Problem 1: Given the nonlinear relation (4) for estimation of the MOoP, find estimates for $\hat{U}_i(t)$ (BEWS) and $\hat{\bar{U}}(t)$ (REWS).

The following subsections outline two wind speed estimation techniques. The last subsection concludes by performing a similarity analysis.

A. Proportional-Integral-Notch Estimator

In our previous work [4], the widely-used I&I estimator was revisited by extending the proportional-only structure with an integral correction term. Inspired by the extended I&I estimator which returns an estimate of the REWS, this letter proposes a novel wind speed estimator called the proportional-integral-notch (PIN) estimator to estimate the BEWS. The frequency content of the wind speed experienced by each blade is composed of specific harmonics that are related to (integer multiples of) the rotor rotational frequency, often denoted as nP. This is due to, e.g., the wind shear and tower shadow. The BEWS can thus be estimated by amplifying those specific frequencies via a feedback control structure. Therefore, the periodic wind speed over an individual blade i can be estimated as

$$\begin{cases} \epsilon_i = m_i - \hat{m}_i\Big(\omega_\mathrm{r}, \hat{U}_i, \hat{q}_i, \psi_i\Big) \\ \hat{U}_i(s) = K(s)\epsilon_i(s) = \big(k_\mathrm{p} K_\mathrm{N}(s) + k_\mathrm{i}/s\big)\epsilon_i, \end{cases} \tag{5}$$

where $\{k_\mathrm{p}, k_\mathrm{i}\} \in \mathbb{R}^+$ are the proportional and integral gains. The error between the estimated and measured MOoP is indicated by ϵ_i. The notch transfer function $K_\mathrm{N}(s)$ is scheduled by the rotor speed ω_r and is defined as:

$$K_\mathrm{N}(s) = \frac{2\omega_\mathrm{r} s}{s^2 + \omega_\mathrm{r}^2}. \tag{6}$$

As a result, the PIN estimator transfer matrix $C_\mathrm{PIN}(s, \omega_\mathrm{r})$ is formulated as:

$$\begin{bmatrix} \hat{U}_1(s) \\ \hat{U}_2(s) \\ \hat{U}_3(s) \end{bmatrix} := \underbrace{\begin{bmatrix} K(s) & 0 & 0 \\ 0 & K(s) & 0 \\ 0 & 0 & K(s) \end{bmatrix}}_{C_\mathrm{PIN}(s,\omega_\mathrm{r})} \begin{bmatrix} \epsilon_1(s) \\ \epsilon_2(s) \\ \epsilon_3(s) \end{bmatrix}. \tag{7}$$

From Eq. (7), it is evident that a diagonal and decoupled BEWS estimator $K(s)$ solely responds to its local blade load measurements as depicted in Fig. 2(a). However, it is well known that there exists a significant amount of dynamic coupling between the blades of a turbine rotor [10], that is, the coupling is present between the wind speed $\hat{U}_i(s)$ and the blade load $m_j(s)$ for $i \neq j$. The PIN estimator $C_\mathrm{PIN}(s, \omega_\mathrm{r})$ is diagonal and thus the off-diagonal terms are nonexistent, which implies that the proposed estimator is unable to take the coupling effects between blades into account.

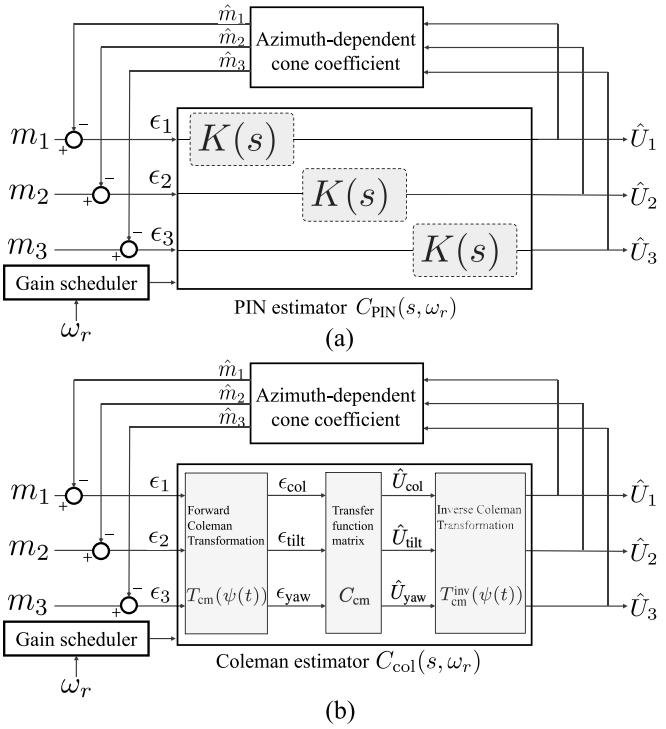

Fig. 2. Block diagram of the BEWS estimators formed by a negative feedback interconnection of a linear estimator and a nonlinear azimuth-dependent cone coefficient. (a) PIN estimator, (b) Coleman estimator.

The lack of information on the coupled blade dynamics will degrade the performance of the wind speed estimator, as will become apparent during the numerical simulations in Section IV. To cope with the problem of unmodeled dynamics, we propose a second estimation technique which employs the Coleman transformation in a similar estimation framework. This will be outlined in the next subsection. Afterwards, the resemblances between and differences of both estimators are discussed.

B. Coleman Estimator

The Coleman transformation [12] is an important technique to convert rotating wind turbine dynamics into a nonrotating reference frame. By replacing the diagonal part of the PIN estimator with the forward and inverse Coleman transformations and by including a diagonal integral transfer matrix, the so-called Coleman estimator is formulated as shown in Fig. 2(b).

The forward Coleman transformation used in the estimator is defined as follows:

$$\begin{bmatrix} \epsilon_\mathrm{col} \\ \epsilon_\mathrm{tilt} \\ \epsilon_\mathrm{yaw} \end{bmatrix} := \underbrace{\frac{2}{3}\begin{bmatrix} 1/2 & 1/2 & 1/2 \\ \cos(\psi_1) & \cos(\psi_2) & \cos(\psi_3) \\ \sin(\psi_1) & \sin(\psi_2) & \sin(\psi_3) \end{bmatrix}}_{T_\mathrm{cm}(\psi(t))} \begin{bmatrix} \epsilon_1 \\ \epsilon_2 \\ \epsilon_3 \end{bmatrix}, \tag{8}$$

where ϵ_tilt and ϵ_yaw are the error signals of the estimated and projected MOoP in tilt and yaw directions, respectively, while ϵ_col indicates that of the collective MOoP estimation.

With the following transfer function matrix – composed out of pure integrals in a diagonal structure – the quantities above

are mapped to the estimated collective, tilt and yaw wind speed components in the nonrotating frame:

$$\begin{bmatrix}\hat{U}_{\text{col}}\\ \hat{U}_{\text{tilt}}\\ \hat{U}_{\text{yaw}}\end{bmatrix} := \underbrace{\begin{bmatrix}K_{\text{col}}/s & 0 & 0\\ 0 & K_0/s & 0\\ 0 & 0 & K_0/s\end{bmatrix}}_{C_{\text{cm}}(s)}\begin{bmatrix}\epsilon_{\text{col}}\\ \epsilon_{\text{tilt}}\\ \epsilon_{\text{yaw}}\end{bmatrix}, \tag{9}$$

where K_{col} is the integral gain for estimating the collective component of the wind speed. As will be shown later, the equal gain K_0 for both the tilt and yaw referred wind speeds, is a necessary condition. Finally, the signals are projected back into the rotating frame to obtain BEWS with the inverse Coleman transformation

$$\begin{bmatrix}\hat{U}_1\\ \hat{U}_2\\ \hat{U}_3\end{bmatrix} := \underbrace{\begin{bmatrix}1 & \cos(\psi_1) & \sin(\psi_1)\\ 1 & \cos(\psi_2) & \sin(\psi_2)\\ 1 & \cos(\psi_3) & \sin(\psi_3)\end{bmatrix}}_{T_{\text{cm}}^{\text{inv}}(\psi(t))}\begin{bmatrix}\hat{U}_{\text{col}}\\ \hat{U}_{\text{tilt}}\\ \hat{U}_{\text{yaw}}\end{bmatrix}. \tag{10}$$

C. Similarities Between the PIN and the Coleman Estimators

Given the two seeming dissimilar BEWS estimators, it is compelling to attempt to understand their similarities. To achieve this goal, the Toeplitz matrix of the Coleman estimator gain is first derived in Proposition 1.

Proposition 1: Let us consider the wind turbine operating at a constant rotor speed, that is, $\dot{\omega}_{\text{r}}(t) = 0$. The Coleman estimator gain C_{col} consisting of Eqs. (8), (9) and (10) is equivalent to the following Toeplitz matrix:

$$C_{\text{col}}(s, \omega_{\text{r}}) := \begin{bmatrix}K_{\text{R,a}}(s) & K_{\text{R,b}}(s) & K_{\text{R,c}}(s)\\ K_{\text{R,c}}(s) & K_{\text{R,a}}(s) & K_{\text{R,b}}(s)\\ K_{\text{R,b}}(s) & K_{\text{R,c}}(s) & K_{\text{R,a}}(s)\end{bmatrix}, \tag{11}$$

where the subscript '*R*' indicates the rotating reference frame, and the transfer functions $K_{\text{R,a}}$, $K_{\text{R,b}}$ and $K_{\text{R,c}}$ are defined as:

$$K_{\text{R,a}}(s) := \frac{(2K_0 + K_{\text{col}})s^2 + K_{\text{col}}\omega_{\text{r}}^2}{3s(s^2 + \omega_r^2)},$$

$$K_{\text{R,b}}(s) := \frac{(K_{\text{col}} - K_0)s^2 + (K_0\sqrt{3}\omega_{\text{r}})s + K_{\text{col}}\omega_{\text{r}}^2}{3s(s^2 + \omega_r^2)},$$

$$K_{\text{R,c}}(s) := \frac{(K_{\text{col}} - K_0)s^2 - (K_0\sqrt{3}\omega_{\text{r}})s + K_{\text{col}}\omega_{\text{r}}^2}{3s(s^2 + \omega_r^2)}.$$

Proof: Given the constant ω_{r}, the transfer function between $\hat{U}_{\text{col,tilt,yaw}}(s)$ and $\hat{U}_{1,2,3}(s)$ is then formulated as:

$$\begin{bmatrix}\hat{U}_1(s)\\ \hat{U}_2(s)\\ \hat{U}_3(s)\end{bmatrix} = \mathcal{C}_-^{\text{T}}\begin{bmatrix}\hat{U}_{\text{col}}(s - \text{j}\omega_{\text{r}})\\ \hat{U}_{\text{tilt}}(s - \text{j}\omega_{\text{r}})\\ \hat{U}_{\text{yaw}}(s - \text{j}\omega_{\text{r}})\end{bmatrix} + \mathcal{C}_+^{\text{T}}\begin{bmatrix}\hat{U}_{\text{col}}(s + \text{j}\omega_{\text{r}})\\ \hat{U}_{\text{tilt}}(s + \text{j}\omega_{\text{r}})\\ \hat{U}_{\text{yaw}}(s + \text{j}\omega_{\text{r}})\end{bmatrix} + \mathcal{C}_{\text{col}}^{\text{T}}\begin{bmatrix}\hat{U}_{\text{col}}(s)\\ \hat{U}_{\text{tilt}}(s)\\ \hat{U}_{\text{yaw}}(s)\end{bmatrix}, \tag{12}$$

where

$$\mathcal{C}_- = \frac{1}{2}\begin{bmatrix}0 & 0 & 0\\ 0 & 1 & \text{j}\\ 0 & -\text{j} & 1\end{bmatrix}\begin{bmatrix}0 & 0 & 0\\ \cos(0) & \cos(\frac{2\pi}{3}) & \cos(\frac{4\pi}{3})\\ \sin(0) & \sin(\frac{2\pi}{3}) & \sin(\frac{4\pi}{3})\end{bmatrix},$$

$$\mathcal{C}_+ = \frac{1}{2}\begin{bmatrix}0 & 0 & 0\\ 0 & 1 & -\text{j}\\ 0 & \text{j} & 1\end{bmatrix}\begin{bmatrix}0 & 0 & 0\\ \cos(0) & \cos(\frac{2\pi}{3}) & \cos(\frac{4\pi}{3})\\ \sin(0) & \sin(\frac{2\pi}{3}) & \sin(\frac{4\pi}{3})\end{bmatrix},$$

and

$$\mathcal{C}_{\text{col}} = \begin{bmatrix}1 & 1 & 1\\ 0 & 0 & 0\\ 0 & 0 & 0\end{bmatrix},$$

with $\text{j} = \sqrt{-1}$ being the imaginary unit. Given the diagonal integral form of Eq. (9), the frequency-shifted transfer function is derived as:

$$\begin{bmatrix}\hat{U}_{\text{col}}(s - \text{j}\omega_{\text{r}})\\ \hat{U}_{\text{tilt}}(s - \text{j}\omega_{\text{r}})\\ \hat{U}_{\text{yaw}}(s - \text{j}\omega_{\text{r}})\end{bmatrix} = C_{\text{cm}}(s - \text{j}\omega_{\text{r}})\begin{bmatrix}\epsilon_{\text{col}}(s - \text{j}\omega_{\text{r}})\\ \epsilon_{\text{tilt}}(s - \text{j}\omega_{\text{r}})\\ \epsilon_{\text{yaw}}(s - \text{j}\omega_{\text{r}})\end{bmatrix}, \tag{13}$$

and

$$\begin{bmatrix}\hat{U}_{\text{col}}(s + \text{j}\omega_{\text{r}})\\ \hat{U}_{\text{tilt}}(s + \text{j}\omega_{\text{r}})\\ \hat{U}_{\text{yaw}}(s + \text{j}\omega_{\text{r}})\end{bmatrix} = C_{\text{cm}}(s + \text{j}\omega_{\text{r}})\begin{bmatrix}\epsilon_{\text{col}}(s + \text{j}\omega_{\text{r}})\\ \epsilon_{\text{tilt}}(s + \text{j}\omega_{\text{r}})\\ \epsilon_{\text{yaw}}(s + \text{j}\omega_{\text{r}})\end{bmatrix}. \tag{14}$$

Combining Eqs. (13) and (14), Eq. (12) is rewritten as:

$$\begin{bmatrix}\hat{U}_1(s)\\ \hat{U}_2(s)\\ \hat{U}_3(s)\end{bmatrix} = \mathcal{C}_-^{\text{T}}C_{\text{cm}}(s - \text{j}\omega_{\text{r}})\begin{bmatrix}\epsilon_{\text{col}}(s - \text{j}\omega_{\text{r}})\\ \epsilon_{\text{tilt}}(s - \text{j}\omega_{\text{r}})\\ \epsilon_{\text{yaw}}(s - \text{j}\omega_{\text{r}})\end{bmatrix} + \mathcal{C}_+^{\text{T}}C_{\text{cm}}(s + \text{j}\omega_{\text{r}})\begin{bmatrix}\epsilon_{\text{col}}(s + \text{j}\omega_{\text{r}})\\ \epsilon_{\text{tilt}}(s + \text{j}\omega_{\text{r}})\\ \epsilon_{\text{yaw}}(s + \text{j}\omega_{\text{r}})\end{bmatrix} + \mathcal{C}_{\text{col}}^{\text{T}}C_{\text{cm}}(s)\begin{bmatrix}\epsilon_{\text{col}}(s)\\ \epsilon_{\text{tilt}}(s)\\ \epsilon_{\text{yaw}}(s)\end{bmatrix}. \tag{15}$$

In addition, the Coleman transformed expressions of $\epsilon_{1,2,3}$ are formulated in the frequency domain as:

$$\begin{bmatrix}\epsilon_{\text{col}}(s)\\ \epsilon_{\text{tilt}}(s)\\ \epsilon_{\text{yaw}}(s)\end{bmatrix} = \frac{2}{3}\mathcal{C}_-\begin{bmatrix}\epsilon_1(s - \text{j}\omega_{\text{r}})\\ \epsilon_2(s - \text{j}\omega_{\text{r}})\\ \epsilon_3(s - \text{j}\omega_{\text{r}})\end{bmatrix} + \frac{2}{3}\mathcal{C}_+\begin{bmatrix}\epsilon_1(s + \text{j}\omega_{\text{r}})\\ \epsilon_2(s + \text{j}\omega_{\text{r}})\\ \epsilon_3(s + \text{j}\omega_{\text{r}})\end{bmatrix} + \frac{1}{3}\mathcal{C}_{\text{col}}\begin{bmatrix}\epsilon_1(s)\\ \epsilon_2(s)\\ \epsilon_3(s)\end{bmatrix}. \tag{16}$$

Now, substituting Eq. (16) into Eq. (15) yields

$$\begin{aligned}\begin{bmatrix}\hat{U}_1(s)\\ \hat{U}_2(s)\\ \hat{U}_3(s)\end{bmatrix} &= \mathcal{C}_-^{\text{T}}C_{\text{cm}}(s - \text{j}\omega_{\text{r}})\\ &\times\left(\frac{2}{3}\mathcal{C}_-\begin{bmatrix}\epsilon_1(s - 2\text{j}\omega_{\text{r}})\\ \epsilon_2(s - 2\text{j}\omega_{\text{r}})\\ \epsilon_3(s - 2\text{j}\omega_{\text{r}})\end{bmatrix} + \frac{2}{3}\mathcal{C}_+\begin{bmatrix}\epsilon_1(s)\\ \epsilon_2(s)\\ \epsilon_3(s)\end{bmatrix} + \frac{1}{3}\mathcal{C}_{\text{col}}\begin{bmatrix}\epsilon_1(s - \text{j}\omega_{\text{r}})\\ \epsilon_2(s - \text{j}\omega_{\text{r}})\\ \epsilon_3(s - \text{j}\omega_{\text{r}})\end{bmatrix}\right)\\ &+ \mathcal{C}_+^{\text{T}}C_{\text{cm}}(s + \text{j}\omega_{\text{r}})\left(\frac{2}{3}\mathcal{C}_-\begin{bmatrix}\epsilon_1(s)\\ \epsilon_2(s)\\ \epsilon_3(s)\end{bmatrix} + \frac{2}{3}\mathcal{C}_+\begin{bmatrix}\epsilon_1(s + 2\text{j}\omega_{\text{r}})\\ \epsilon_2(s + 2\text{j}\omega_{\text{r}})\\ \epsilon_3(s + 2\text{j}\omega_{\text{r}})\end{bmatrix}\right.\\ &\left. + \frac{1}{3}\mathcal{C}_{\text{col}}\begin{bmatrix}\epsilon_1(s + \text{j}\omega_{\text{r}})\\ \epsilon_2(s + \text{j}\omega_{\text{r}})\\ \epsilon_3(s + \text{j}\omega_{\text{r}})\end{bmatrix}\right)\\ &+ \mathcal{C}_{\text{col}}^{\text{T}}C_{\text{cm}}(s)\left(\frac{2}{3}\mathcal{C}_-\begin{bmatrix}\hat{U}_1(s - \text{j}\omega_{\text{r}})\\ \hat{U}_2(s - \text{j}\omega_{\text{r}})\\ \hat{U}_3(s - \text{j}\omega_{\text{r}})\end{bmatrix} + \frac{2}{3}\mathcal{C}_+\begin{bmatrix}\epsilon_1(s + \text{j}\omega_{\text{r}})\\ \epsilon_2(s + \text{j}\omega_{\text{r}})\\ \epsilon_3(s + \text{j}\omega_{\text{r}})\end{bmatrix} + \frac{1}{3}\mathcal{C}_{\text{col}}\begin{bmatrix}\epsilon_1(s)\\ \epsilon_2(s)\\ \epsilon_3(s)\end{bmatrix}\right).\end{aligned} \tag{17}$$

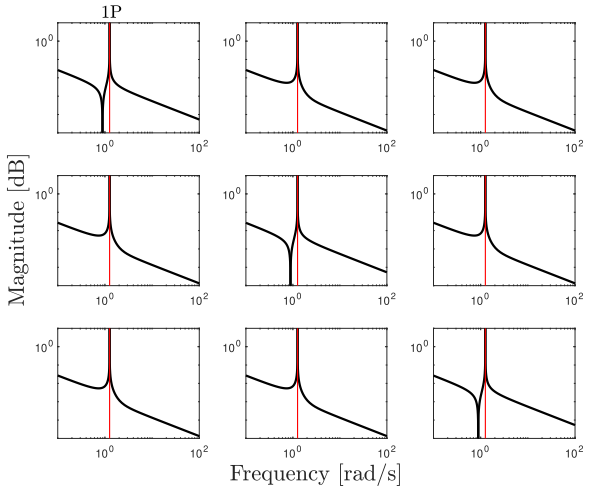

Fig. 3. Bode magnitude plots of the Coleman estimator defined by the transfer function matrix in Eq. (11), where 1P frequency is assumed as constant, which is indicated by a red vertical line.

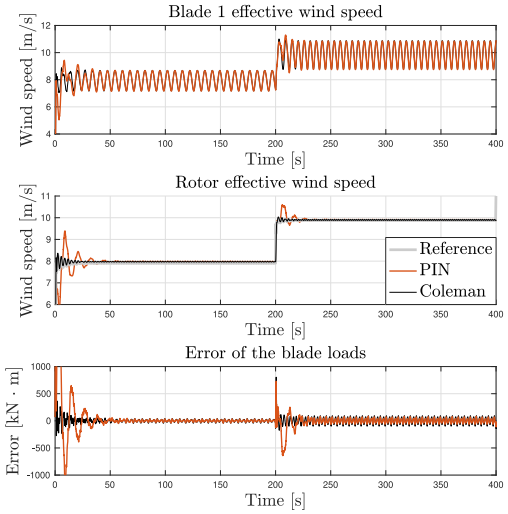

Fig. 4. Time traces of the wind speed and the estimation error on blade 1 between the PIN and the Coleman estimators under the step-wise sheared wind condition. Blades 2-3 show similar results and hence omitted.

Given an equal gain K_0 for the tilt and yaw wind speed estimate contributions in Eq. (9), Eq. (17) can be simplified by the remarkable property:

$$\mathcal{C}_-^{\mathrm{T}}\mathcal{C}_- = \mathcal{C}_+^{\mathrm{T}}\mathcal{C}_+ = \mathcal{C}_-^{\mathrm{T}}\mathcal{C}_{\mathrm{col}} = \mathcal{C}_+^{\mathrm{T}}\mathcal{C}_{\mathrm{col}} = \mathcal{C}_{\mathrm{col}}^{\mathrm{T}}\mathcal{C}_- = \mathcal{C}_{\mathrm{col}}^{\mathrm{T}}\mathcal{C}_+ = 0,$$

giving rise to the following equation:

$$\begin{bmatrix}\hat{U}_1(s)\\ \hat{U}_2(s)\\ \hat{U}_3(s)\end{bmatrix} = \Big(\frac{2}{3}\mathcal{C}_-^{\mathrm{T}}C_{\mathrm{cm}}(s-\mathrm{j}\omega_{\mathrm{r}})\mathcal{C}_+ + \frac{2}{3}\mathcal{C}_+^{\mathrm{T}}C_{\mathrm{cm}}(s+\mathrm{j}\omega_{\mathrm{r}})\mathcal{C}_- + \frac{1}{3}\mathcal{C}_{\mathrm{col}}^{\mathrm{T}}C_{\mathrm{cm}}(s)\mathcal{C}_{\mathrm{col}}\Big)\begin{bmatrix}\epsilon_1(s)\\ \epsilon_2(s)\\ \epsilon_3(s)\end{bmatrix}, \tag{18}$$

which results in the Toeplitz matrix of the proposed Coleman estimator and completes the proof. ■

Bode magnitude plots of the transfer function matrix $C_{\mathrm{col}}(s,\omega_{\mathrm{r}})$ are illustrated in Fig. 3, where $\omega_{\mathrm{r}} = 2\pi f_r$ with $f_r = 0.2$ Hz refers to a constant once-per-revolution (1P) angular frequency of the considered wind turbine model.

The similarities between the PIN estimator (Eq. (7)) and the Coleman estimator (Eq. (11)) are now further illustrated in the frequency domain.

Theorem 1: Consider the wind turbine operating at a constant rotor speed, that is, $\dot{\omega}_{\mathrm{r}}(t) = 0$. Given the nonlinear and azimuth-dependent cone coefficient of Eq. (1), $C_{\mathrm{PIN}}(s,\omega_{\mathrm{r}})$ defined in Eq. (7) is equivalent to a diagonal structure of $C_{\mathrm{col}}(s)$ in Eq. (11) only including $K_{\mathrm{R,a}}(s)$, where

$$k_{\mathrm{i}} = \frac{K_{\mathrm{col}}}{3}, \qquad k_{\mathrm{p}} = \frac{K_0}{3\omega_{\mathrm{r}}}. \tag{19}$$

Proof: To prove Theorem 1, the equality $K(s) = K_{\mathrm{R,a}}(s)$ needs to hold under the conditions of Eq. (19). It is known from Eqs. (5) and (6) that

$$K(s) = k_{\mathrm{p}}\frac{2\omega_{\mathrm{r}}s}{s^2+\omega_{\mathrm{r}}^2} + \frac{k_{\mathrm{i}}}{s} \tag{20}$$

$$= \frac{k_{\mathrm{p}}s}{s}\frac{2\omega_{\mathrm{r}}s}{s^2+\omega_{\mathrm{r}}^2} + \frac{k_{\mathrm{i}}}{s}\frac{s^2+\omega_{\mathrm{r}}^2}{s^2+\omega_{\mathrm{r}}^2} \tag{21}$$

$$= \frac{(2k_{\mathrm{p}}\omega_{\mathrm{r}}+k_{\mathrm{i}})s^2 + k_{\mathrm{i}}\omega_{\mathrm{r}}^2}{s(s^2+\omega_{\mathrm{r}}^2)}. \tag{22}$$

Given condition (19), it is evident that Eq. (22) is equal to $K_{\mathrm{R,a}}$ in (11) which proves that the PIN estimator is equivalent to a particular diagonal structure of the Coleman estimator. ■

IV. Case Study

This section performs a case study to verify the theoretical analysis and to demonstrate the similarities between the PIN and the Coleman estimators.

NREL's high-fidelity wind turbine simulation software package Fatigue, Aerodynamics, Structures, and Turbulence (FAST) [13] is utilized to simulate the wind turbine dynamics. The closed-loop control system including both wind speed estimator types is implemented in Simulink. The baseline *K-omega-squared* torque control law [11], with a predefined optimal mode gain, is used in this letter. To evaluate the performance of the estimators, a sheared wind profile with a step-wise increasing wind speed from 8 m/s to 10 m/s and a turbulent wind flow with an ambient wind speed of 8 m/s and turbulence intensity of 15 % are considered. The simulation time step is set to 0.01 s.

The estimation results of the PIN and Coleman estimators are presented in Figs. 4–5, where the BEWS, the REWS and the estimation error of the blade loads are illustrated successively for comparisons. The proposed estimators show similar results for both step-wise sheared and turbulent wind conditions, which substantiates Theorem 1. The power spectra of the estimated step-wise sheared wind speed calculated for 200 s – 400 s are presented in Fig. 6. The spectrum of the actual rotor effective wind speed computed by FAST is included as a reference and benchmark to evaluate the estimator performance. The Coleman and PIN estimators show almost consistent performance for the dominant 1P harmonic. For the other frequencies, the power spectrum of the Coleman estimator is closer to the reference value. This indicates that, compared to the PIN estimator, the Coleman estimator has a

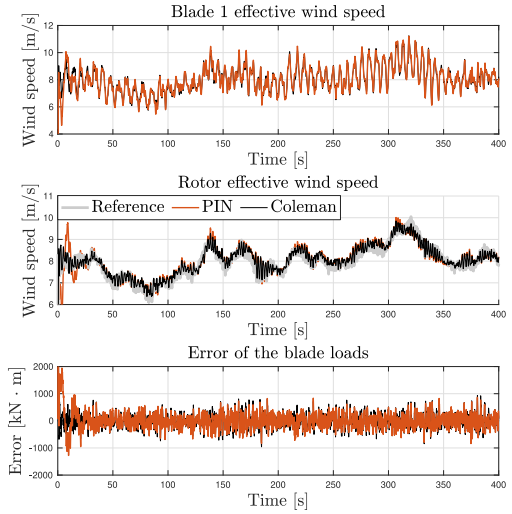

Fig. 5. Time traces of the wind speed and the estimation error on blade 1 between the PIN and the Coleman estimators under the turbulent wind condition. Blades 2-3 show similar results and are omitted.

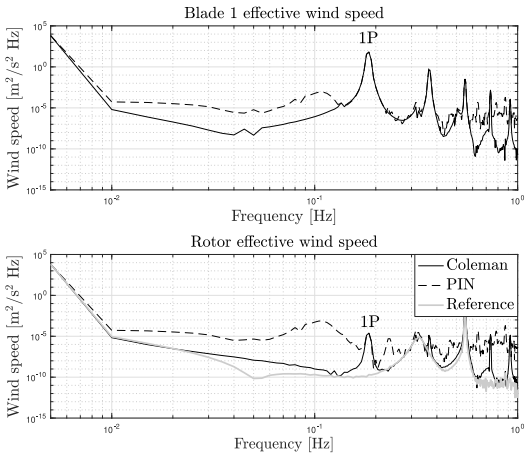

Fig. 6. Simulation results on the NREL 5MW wind turbine under step-wise sheared wind conditions. The power spectrum of the wind speed on blade 1 illustrates the performance similarities between the PIN and the Coleman estimators. Blades 2-3 show similar results and hence omitted.

superior estimation quality for non-1P frequencies. In addition, it is evident that the Coleman estimator shows less oscillations during transients than the PIN estimator, which leads to a smoother and faster tracking of the actual wind speed. Such a smoother transient response is explained by Eq. (11), as the MIMO transmission zeros are canceled in this full transfer function matrix form. The power spectrum under the turbulent wind condition shows similar results, and is hence omitted for brevity.

In summary, both wind speed estimators show similar performance for the considered step-wise sheared and turbulent wind conditions, which verifies Theorem 1. Since the effects of the transmission zeros are eliminated, the Coleman estimator exhibits a smoother transient response than the PIN estimator.

V. Conclusion

Two novel blade effective wind speed (BEWS) estimation schemes are proposed and an analysis is performed on the similarities of both implementations. First, a proportional-integral-notch (PIN) estimator is introduced, which is formed by a negative feedback interconnection of a linear diagonally decoupled estimator and a nonlinear azimuth-dependent cone coefficient. Following the same philosophy, a Coleman estimator, which is based on the Coleman transformation, is developed to incorporate the coupled rotor dynamics into the estimation scheme.

Given the seeming disparities between these two estimators, it is proven that there exists structural and performance similarities between the PIN and the Coleman estimators. Analytical and numerical results show the diagonal PIN and coupled Coleman estimators exhibit similar estimation results. In particular, the PIN estimator, which is considered as a diagonal form of the Coleman estimator, is a simple but effective method to estimate the BEWS. The Coleman estimator, on the other hand, is superior in taking into account the coupled rotor dynamics for the BEWS estimation. Since the effects of the MIMO transmission zeros present in the PIN scheme are eliminated by the off-diagonal terms of the Coleman estimator, the latter mentioned shows better transient behavior compared to the PIN estimator.

References

[1] J. Lee and F. Zhao, "Global wind report 2021," Global Wind Energy Council, Brussels, Belgium, Rep., 2021. [Online]. Available: https://gwec.net/wp-content/uploads/2021/03/GWEC-Global-Wind-Report-2021.pdf

[2] M. N. Soltani *et al.*, "Estimation of rotor effective wind speed: A comparison," *IEEE Trans. Control Syst. Technol.*, vol. 21, no. 4, pp. 1155–1167, Jul. 2013.

[3] R. Ortega, F. Mancilla-David, and F. Jaramillo, "A globally convergent wind speed estimator for wind turbine systems," *Int. J. Adapt. Control Signal Process.*, vol. 27, no. 5, pp. 413–425, 2013.

[4] Y. Liu, A. K. Pamososuryo, R. M. G. Ferrari, and J.-W. van Wingerden, "The immersion and invariance wind speed estimator revisited and new results," *IEEE Contr. Syst. Lett.*, vol. 6, pp. 361–366, Apr. 2022. [Online]. Available: https://ieeexplore.ieee.org/document/9416566?source=authoralert

[5] E. Simley and L. Pao, "Correlation between rotating LIDAR measurements and blade effective wind speed," in *Proc. 51st AIAA Aerosp. Sci. Meeting*, 2013, p. 749.

[6] K. Selvam, S. Kanev, J. W. van Wingerden, T. van Engelen, and M. Verhaegen, "Feedback–feedforward individual pitch control for wind turbine load reduction," *Int. J. Robust Nonlinear Control*, vol. 19, no. 1, pp. 72–91, 2009.

[7] G. Goodwin, S. Graebe, and M. Salgado, *Control System Design*. Englewood Cliffs, NJ, USA: Prentice-Hall, 2001.

[8] C. L. Bottasso, S. Cacciola, and J. Schreiber, "Local wind speed estimation, with application to wake impingement detection," *Renew. Energy*, vol. 116, pp. 155–168, Feb. 2018.

[9] Y. Liu, A. K. Pamososuryo, R. Ferrari, T. G. Hovgaard, and J. W. van Wingerden, "Blade effective wind speed estimation: A subspace predictive repetitive estimator approach," in *Proc. Eur. Control Conf. (ECC)*, 2021, pp. 1–6.

[10] S. P. Mulders, A. K. Pamososuryo, G. E. Disario, and J. W. van Wingerden, "Analysis and optimal individual pitch control decoupling by inclusion of an azimuth offset in the multiblade coordinate transformation," *Wind Energy*, vol. 22, no. 3, pp. 341–359, 2019.

[11] J. Jonkman, S. Butterfield, W. Musial, and G. Scott, "Definition of a 5MW reference wind turbine for offshore system development," Nat. Renew. Energy Lab., Golden, CO, USA, Rep. NREL/TP-500-38060, 2009.

[12] G. Bir, "Multi-blade coordinate transformation and its application to wind turbine analysis," in *Proc. 46th AIAA Aerosp. Sci. Meeting Exhibit*, 2008, pp. 1–15.

[13] J. M. Jonkman and M. L. Buhl, Jr., "FAST user's guide," Nat. Renew. Energy Lab., Golden, CO, USA, Rep. NREL/TP-500-38230 (previously NREL/EL-500-29798), 2005.